Inorganic Chemistry

Article

pubs.acs.org/IC

# Metal and Alloy Nanoparticles by Amine-Borane Reduction of Metal Salts by Solid-Phase Synthesis: Atom Economy and Green Process

Udishnu Sanyal and Balaji R. Jagirdar*

Department of Inorganic & Physical Chemistry, Indian Institute of Science, Bangalore 560012, India

Supporting Information

**ABSTRACT:** A new solid state synthetic route has been developed toward metal and bimetallic alloy nanoparticles from metal salts employing amine-boranes as the reducing agent. During the reduction, amine-borane plays a dual role: acts as a reducing agent and reduces the metal salts to their elemental form and simultaneously generates a stabilizing agent in situ which controls the growth of the particles and stabilizes them in the nanosize regime. Employing different amine-boranes with differing reducing ability (ammonia borane (AB), dimethylamine borane (DMAB), and triethylamine borane (TMAB)) was found to have a profound effect on the particle size and the size distribution. Usage of AB as the reducing agent provided the smallest possible size with best size distribution. Employment of TMAB also afforded similar results; however, when DMAB was used as the reducing agent it resulted in larger sized nanoparticles that are polydisperse too. In the AB mediated reduction, $BNH_x$ polymer generated in situ acts as a capping agent whereas, the complexing amine of the other amine-boranes (DMAB and TMAB) play the same role. Employing the solid state route described herein, monometallic Au, Ag, Cu, Pd, and Ir and bimetallic CuAg and CuAu alloy nanoparticles of <10 nm were successfully prepared. Nucleation and growth processes that control the size and the size distribution of the resulting nanoparticles have been elucidated in these systems.

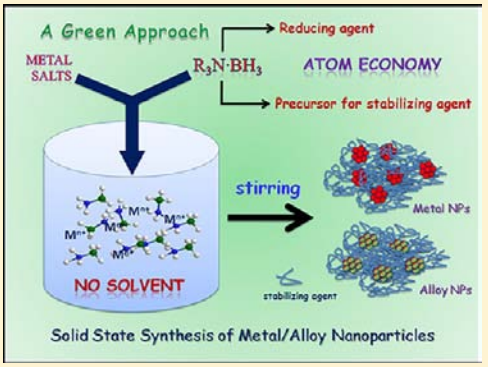


## INTRODUCTION

Conventional methods of synthesis of metal nanoparticles are of two kinds: (a) top-down approach, a physical method involving subdivision of bulk metal into its corresponding nanoparticles and (b) bottom-up approach, employing chemical methods wherein metal ions are reduced to metal atoms in the presence of a stabilizer, followed by controlled aggregation of atoms. Although large scale synthesis of nanoparticles is possible by physical methods, size control is very difficult to achieve in this case. In contrast, the bottom-up approach offers great control over size and shape; however, only subgram quantities could be realized.[1−4] Even being complementary to each other, these methods of synthesis are not sustainable for real time applications. A method of synthesis of metal nanoparticles incorporating aspects of atom economy that can be carried out without any solvent and which is sustainable and has potential applications is highly desirable. In this context, employment of reagents that are capable of playing multiple roles minimizing the number of reagents used in a reaction and hence simplifying and eliminating tedious purification procedures thus bringing out atom economy to the overall process is an attractive prospect. In addition, if the reaction is carried out in the absence of any solvent(s), it adds greenness to the process and could lead to mass production of nanomaterials that are highly sought after for potential applications. Even though it was recognized long ago that "*best solvent is no solvent*" only very few attempts have been made toward this direction.[5−7] For example, Chaudret and his co-workers prepared Ru, Co, and Rh nanoparticles via solid state decomposition under $H_2$ atmosphere of organometallic precursors dispersed in polymer films.[8] A high-speed vibrational milling process for the preparation of Au nanoparticles in a solid state route was developed by Gecekeler et al., wherein $NaBH_4$ was used as the reducing agent and poly-(vinylpyrrolidone) as the stabilizing agent.[9] The particle size could be tuned by varying the reaction time, mass average molar mass of the polymer used as the capping agent, and the mass ratio of the reactants used.

A large body of literature is available on how to achieve control over the particle size as well as size distribution of nanoparticles obtained by the reduction of metal precursors in solution state. By controlling the thermodynamic as well as the kinetic parameters, it is possible to realize nanoparticles of desired size with very narrow size distribution ($\sigma \leq 5\%$).[10] On the other hand, barring few isolated examples, solid phase synthesis of metal nanoparticles remains largely unexplored. This is primarily due to a lack of fundamental understanding of the formation mechanism (i.e., nucleation and growth) of monodisperse nanoparticles in the solid phase in comparison to their solution state equivalent. Effect of the thermodynamic and the kinetic parameters on the size and the size distribution of particles obtained in a solid state route via reduction of metal precursor using a reducing agent are not well understood.

**Received:** October 2, 2012
**Published:** November 15, 2012

Bimetallic nanocomposites, on the other hand, have been prepared in solution state by the coreduction of two metal ions which leads to alloy structure. Uniform mixing of two heterogeneous nuclei in the solution state has been identified as a key step in the process leading to alloy formation under ambient conditions. However, to realize the same structure is rather challenging in the solid state because of the poorer mixing of the constituent elements in a heterogeneous mixture. Therefore, harsh reaction conditions, for example, heating at very high temperature is obligatory to realize such structures in the solid state which is detrimental to obtain nanocrystalline bimetallic particles with high surface area necessary for any application. Therefore, an important prerequisite for the development of a sustainable solid state route for metal nanoparticles is a comprehensive understanding of the formation mechanism of the nanoparticles under such conditions.

Among various synthetic methods available for metal nanoparticles, chemical methods are the most attractive because of their simplicity and propensity to produce monodisperse nanoparticles. In this direction, amine-boranes have found great use for the organic chemists and have attracted immense interest from the standpoint of hydrogen storage.[11] They are also tipped as one of the most promising and sustainable reducing agents because of their mild reducing nature and capability to play multiple roles. The potential advantages of amine-boranes were first explored by Stucky and his co-workers when they developed a single phase method in organic medium and realized highly monodisperse Au, Ag, and AuAg alloy nanoparticles stabilized by dodecanethiol.[12] They also noted that use of different amine-boranes such as tert-butyl amine-, triethyl amine-, morpholine-, and ammonia borane was beneficial over the borohydrides because of their slow kinetics of reduction which helps in achieving much better control over nucleation and growth processes. Variation of the substituent on nitrogen imparts different reducing ability for the amine-borane which is another useful feature of this class of reducing agents. We recently reviewed various aspects of amine-boranes as reducing agents for the synthesis of metal nanoparticles.[13]

In a preliminary communication, we reported the synthesis of monodisperse Au, Ag, and air-stable Cu nanoparticles in a solid state route using $H_3N{\cdot}BH_3$ (AB), a classical Lewis acid–base adduct.[14] In this novel synthetic procedure, AB serves a dual purpose: it acts as a reducing agent to reduce the metal precursor to generate the nuclei and simultaneously undergoes decomposition to furnish $BNH_x$ polymer in which the metal nanoparticles get embedded. This in turn, prevents aggregation of metal nanoparticles and stabilizes them in the nanosize regime. Though AB has been used as a reducing agent in solution state,[15−18] its reducing ability in the solid state is still underdeveloped. As a follow up of our previous communication, we elaborated our solid state synthetic route to other metal and alloy nanoparticles to gain comprehensive understanding on their formation mechanisms. In addition, we also attempted to examine the rate of reduction of the metal salts by employing amine-boranes that vary in their reducing ability, for example, ammonia borane, $H_3N{\cdot}BH_3$ (AB), dimethylamine borane, $Me_2HN{\cdot}BH_3$ (DMAB), and trimethylamine borane, $Me_3N{\cdot}BH_3$ (TMAB). The reducing ability of these amine-boranes follows the order: AB > DMAB > TMAB.[19] We also attempted to extend our synthetic protocol to bimetallic systems. The results of these studies are presented herein.

## EXPERIMENTAL SECTION

**Materials.** Ammonia borane ($H_3N{\cdot}BH_3$, AB) was synthesized from $(NH_4)_2SO_4$ and $NaBH_4$ using the procedure reported by Ramachandran and Gagare.[20] Dimethylamine borane ($Me_2HN{\cdot}BH_3$, DMAB) and trimethylamine borane ($Me_3N{\cdot}BH_3$, TMAB) were purchased from Sigma Aldrich and used as received. The metal salts $CuCl_2{\cdot}2H_2O$, $Cu(NO_3)_2$, $AgNO_3$, $HAuCl_4$, $H_2IrCl_6$, and $Pd(OCOCH_3)_2$ were obtained from S. D. Fine Chemicals Limited, India. Anhydrous $CuCl_2$ was obtained by heating the hydrous salt at 100 °C under vacuum for 12 h.

**Instrumentation.** The TEM bright field (BF) images, selected area electron diffraction (SAED) patterns, high resolution TEM (HRTEM) images, and the high-angle annular dark field (HAADF) images were acquired using a TECNAI T20 transmission electron microscope and JEOL 2100F field emission transmission electron microscope, both operating at 200 kV and TECNAI F30 FETEM operating at 300 kV. To prepare the TEM samples, the metal nanopowder was first redispersed in tetrahydrofuran (THF) by sonication for about 15 min and then 2 $\mu$L of this solution was placed on a carbon coated copper grid and finally dried under a lamp. In case of Cu/Au bimetallic nanoparticles, samples were prepared on Ni grids whereas Au grids were used for imaging Cu/Ag bimetallic nanoparticles. Powder X-ray diffraction measurements were carried out using a Bruker D8 ADVANCE and Philips Xpert powder X-ray diffractometers using Cu $K_\alpha$ radiation. X-ray photoelectron spectra (XPS) were recorded using a Thermoscientific Multilab 2000 instrument. Binding energies reported are with reference to C (1s) at 284.5 eV and are accurate within ±0.1 eV. The FTIR spectra were recorded using a Bruker ALPHA FTIR spectrometer working in the 400−4000 $cm^{-1}$ range.

**Preparation of Ag Nanoparticles.** In a typical experiment, 77 mg of AB (2.5 mmol) was taken in a Schlenk tube and inserted into an oil bath preheated to and maintained at 60 °C. Silver nitrate, $AgNO_3$ (85 mg, 0.5 mmol) was added to the Schlenk tube in a batch-wise manner (~5 mg in each batch under $N_2$ atmosphere) and vigorously stirred. In our previous communication,[14] we employed AB to metal salt ratio at 10, but we found that the reaction works quite well at a ratio of 5 itself. During the addition of $AgNO_3$ to AB, a small flame accompanied by evolution of white fumes was noted. The color of the reaction mixture turned yellow from colorless. When the addition of the metal salt was complete, the reaction mixture was stirred for 3 h to ensure that the reaction went to completion. Then the powders were isolated and washed 6 to 7 times using dry THF and dried under vacuum. The final powder samples that were obtained were dark yellow and were used as such for powder XRD. The TEM samples were made from this powder by redispersing in THF via sonication.

In a similar manner, DMAB was used to prepare Ag nanoparticles in the solid state. In a typical experiment, 147 mg of DMAB (2.5 mmol) was taken in a Schlenk tube, and it was immersed in an oil bath preheated and maintained at 60 °C. Silver nitrate, $AgNO_3$ (85 mg, 0.5 mmol), was then added in a batch-wise manner (~5 mg in each batch under $N_2$ atmosphere), and the reaction mixture was vigorously stirred for 3 h. As the melting point of DMAB is 37 °C, the mixture appeared to be semisolid. The color of the final powder was dark yellow. It was washed with dry THF several times and used for further characterization.

In case of preparation of Ag nanoparticles using TMAB, 182 mg (2.5 mmol) of TMAB was placed in a Schlenk tube, and 85 mg (0.5 mmol) of $AgNO_3$ was added to it in a batch-wise manner under vigorous stirring. The reaction was performed at room temperature since TMAB sublimes at 60 °C. The reaction did not proceed to completion within 3 h as in the above cases because TMAB is a weaker reducing agent in comparison to AB and DMAB. The reaction mixture was stirred for 12 h after which time, it was complete. The color of the nanopowder obtained in this case was also dark yellow.

***Caution!*** *Addition of $AgNO_3$ to AB and DMAB was found to be highly exothermic and results in a fire during the reduction process. Therefore, extreme care should be exercised during the reaction; most importantly, addition of bulk amounts of $AgNO_3$ to AB or DMAB should not be done.*


dx.doi.org/10.1021/ic3021436 | Inorg. Chem. 2012, 51, 13023−13033

**Preparation of Au Nanoparticles.** Gold nanoparticles were prepared starting from 46 mg of AB (1.5 mmol) or DMAB (88 mg, 1.5 mmol) or TMAB (109 mg, 1.5 mmol) and $HAuCl_4$ (102 mg, 0.3 mmol) in a similar manner to that of Ag nanoparticles. The yellow colored reaction mixture turned dark red. This dark red nanopowder of Au was washed with THF several times, dried under vacuum and then used for further characterization.

**Preparation of Cu Nanoparticles.** Copper nanoparticles were also prepared in a similar manner to that of Ag nanoparticles, starting from AB (77 mg, 2.5 mmol) or DMAB (147 mg, 2.5 mmol) and anhydrous $CuCl_2$ (67 mg, 0.5 mmol). The color of the reaction mixture turned from brown to red in the reaction with AB; in case of the reaction with DMAB, the brown colored reaction mixture turned gradually brick red almost after 10 min. No further color change was noted even after long reaction time (~6−7 h). As TMAB is a very weak reducing agent, reduction of Cu ions to its elemental state did not take place (amount of TMAB used: 182 mg, 2.5 mmol).

**Preparation of Pd Nanoparticles.** Palladium nanoparticles were prepared in a manner similar to that of Ag starting from AB (77 mg, 2.5 mmol) or DMAB (147 mg, 2.5 mmol) or TMAB (182 mg, 2.5 mmol) and palladium acetate, $Pd(OCOCH_3)_2$ (112 mg, 0.5 mmol). The color of the reaction mixture upon addition of $Pd(OCOCH_3)_2$ was black. The black nanopowder was washed several times with THF, dried in vacuo, and used for further characterization.

**Preparation of Ir Nanoparticles.** Iridium nanoparticles were prepared in a similar manner to that of Ag using AB (77 mg, 2.5 mmol) or DMAB (147 mg, 2.5 mmol) or TMAB (182 mg, 2.5 mmol) and $H_2IrCl_6$ (206 mg, 0.5 mmol). In contrast to earlier cases, no gas evolution or color change of the reaction mixture was noted in the beginning stages of the reaction. The black colored reaction mixture turned yellow almost after 30 min. The reaction was complete in about 6 h when AB or DMAB was used as the reducing agent but took about 12 h when TMAB was used as the reducing agent. The final nanopowder was washed with THF several times and dried and used for further characterization.

**Preparation of Cu/Au Bimetallic Nanoparticles.** In a Schlenk tube was taken 155 mg of AB (5 mmol), and the tube was immersed in an oil bath preheated to and maintained at 60 °C. Copper nitrate, $Cu(NO_3)_2$ (94 mg, 0.5 mmol), and $HAuCl_4$ (170 mg, 0.5 mmol) were mixed thoroughly, and the mixture was added to the Schlenk tube in a batch-wise manner (~5 mg in each batch under $N_2$ atmosphere) while stirring vigorously. The ratio of AB to each metal salt was maintained at 5. During the addition, we noted fire within the tube together with evolution of white fumes accompanied by a color change to reddish brown from yellowish blue. When the addition was complete, the reaction mixture was stirred for 6 h to ensure complete reduction. The powder was then isolated in a similar manner as described above. The isolated powder was red and used as such for powder XRD. The TEM samples were made from this powder by redispersing in THF via sonication.

**Preparation of Cu/Ag Bimetallic Nanoparticles.** Preparation of Cu/Ag bimetallic nanoparticles was carried out in a similar manner to that of Cu/Au nanoparticles. We used copper nitrate, $Cu(NO_3)_2$ (94 mg, 0.5 mmol) and silver nitrate, $AgNO_3$ (85 mg, 0.5 mmol) as the metal precursors and AB (155 mg, 5 mmol) as the reducing agent. In this case as well, the reaction was found to be highly exothermic and resulted in a fire upon addition of metal salts, and the color of the reaction mixture turned black from blue. It was stirred for 6 h within which the reduction was complete, and the final powder obtained was black.

## RESULTS AND DISCUSSION

**1. Effect of Rate of Addition of Metal Salt to Amine-Borane and the Ratio of Amine-Borane to Metal Salt on the Particle Size.** In the preparation of metal nanoparticles via the solid state route, initially amine-borane was taken in a Schlenk tube which was held at 60 °C, and metal salt was added to it under vigorous stirring. We noted that the rate and quantity of addition of metal salt to amine-borane have tremendous influences on the particle size as well as the size distribution. To understand this, we carried out two different sets of reactions. We chose reduction of $AgNO_3$ as the model case. In the first case, $AgNO_3$ was added to AB in a single batch and in the second case, $AgNO_3$ was added in a batch-wise manner (~5 mg per batch with an interval of a few seconds) with vigorous stirring. We earlier reported release of $H_2$ from AB when it is reacted with $Cu^{2+}$ in the solid state.[21] Reactions of metal nitrates with AB in the solid state are quite exothermic; the heat liberated is enough for the hydrogen released to catch fire.

In the first experiment, since reaction of $AgNO_3$ with AB is highly exothermic, sudden addition of entire amount of the silver salt resulted in a big fire and proved to be hazardous. Nevertheless, we carried out the reaction taking adequate precautions and noted a sudden color change from colorless to yellow indicating that the entire amount of $Ag^+$ ions were virtually reduced instantaneously. The TEM BF image of this sample evidenced only agglomerated particles. The selected area electron diffraction (SAED) pattern obtained from one of the agglomerated regions showed a ring pattern corresponding to Ag(0) FCC lattice plane (see Supporting Information).[22]

On the other hand, in the second experiment, $AgNO_3$ was added to AB in small batches. In this case, a gradual color change of the reaction mixture from colorless to yellow was noted. The TEM BF image (see Supporting Information) of this sample revealed the presence of well separated, spherical Ag nanoparticles with a size distribution of 5−10 nm. This could be rationalized taking into account the rate at which the B−N based compound (starting from amine-boranes) is formed after $H_2$ release which acts as a stabilizing agent for the metal nanoparticles during the nucleation process. In the case of AB mediated reduction, it is the $BNH_x$ polymer that is formed simultaneously that provides the stability for the nanoparticles. In this regard, our solid-state route for metal nanoparticles does not require the use of an additional stabilizing agent unlike in instances reported in the literature for the preparation of metal nanoparticles via solid state route using $NaBH_4$ as the reducing agent, wherein a stabilizing agent has been employed.[9] Thus, in the initial stages of reduction when nuclei are formed, there should be adequate amount of polymer matrix present to stabilize the particles effectively. In its absence, uncontrolled growth of particles takes place leading to large particles that are polydisperse and/or agglomerates as well. The rate of metal ion reduction and the rate of polymer matrix formation should be comparable to one another to realize small particles with a narrow size distribution. In this second experiment, wherein metal salt was added to the reducing agent in small batches led to the formation of fewer nuclei which could be capped effectively by the polymer thus restricting them from an uncontrolled growth.

A similar observation was noted when DMAB was used as the reducing agent. However, when TMAB, a much weaker reducing agent compared to AB or DMAB was used,[19] the particle size or the size distribution was unaffected by the manner in which the silver salt was added to the reducing agent. Being a weaker reducing agent, TMAB reduces metal ions very slowly (after almost ~30−45 min a visual color change appeared which darkened gradually signaling the onset of metal ion reduction). Thus even if all the metal salt was added to TMAB in a single batch, the reduction proceeds very slowly and resembles the batch-wise addition of metal salts to AB and DMAB.


dx.doi.org/10.1021/ic3021436 | Inorg. Chem. 2012, 51, 13023−13033

To understand the effect of amine-borane to metal salt ratio on the particle size, we carried out reactions of AB with $HAuCl_4$ wherein the ratio of the reaction mixture was varied systematically. We chose $HAuCl_4$ for these experiments because of its good solubility in THF. Solutions of $HAuCl_4$ in THF are yellow. Reaction progress could be qualitatively monitored in this case by removing a small amount of reaction mixture (powder) at regular time intervals and to it was added THF. If the reaction mixture contains unreacted $HAuCl_4$, the supernatant solution of the resulting solution (with a precipitate) would be yellow. When the reduction had proceeded to completion, addition of THF to the powder gave only a colorless supernatant solution with a precipitate. When AB/$HAuCl_4$ ratios used were 1 and 3, some unreacted $HAuCl_4$ was recovered together with the formation of Au(0) which was evident from the powder XRD pattern (see Supporting Information). Longer reaction time (~24 h) also did not result in completion of the reaction suggesting that the amount of reducing agent taken for the reaction was insufficient. In addition to some unreacted $HAuCl_4$, violet colored Au nanopowders were isolated after 24 h of stirring in both cases. Figure 1a and 1c show the TEM BF images of Au

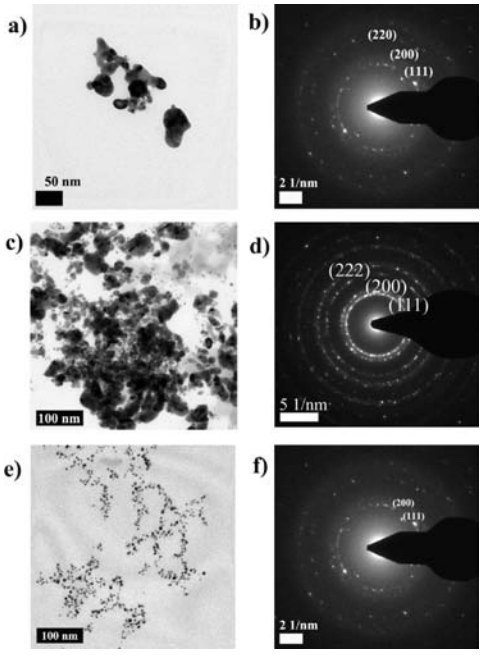


**Figure 1.** Characterization of Au nanoparticles obtained by varying AB/$HAuCl_4$ ratio: (a), (c), (e) TEM BF images; (b), (d), (f) SAED pattern for AB/$HAuCl_4$ (ratio 1, 3, and 5, respectively).

nanoparticles prepared by using AB/$HAuCl_4$ in a ratio of 1 and 3 respectively. These images evidence the presence of only agglomerated particles. The corresponding SAED patterns (Figure 1b and 1d) obtained in both cases showed the presence of rings due to FCC Au(0).[23] In contrast, when the AB/$HAuCl_4$ ratio was maintained at 5 and/or 10, the reaction proceeded to completion within 3 h. The BF TEM image (Figure 1e) of Au nanoparticles obtained from the reaction with AB/$HAuCl_4$ ratio of 5, showed the presence of spherical particles that are embedded in a polymer matrix with a size distribution range of 5−10 nm. We noted a similar observation earlier when we employed a ratio of 10 for AB/$HAuCl_4$.[14] Since no appreciable difference in size of the particles was noted between the two ratios (AB/$HAuCl_4$, 5 and 10), we used AB/metal salt ratio of 5 for the remaining experiments. We also compared the reducing ability of AB at room temperature during the preparation of Au nanoparticles. We attempted to prepare Au nanoparticles at room temperature wherein AB to $HAuCl_4$ ratio was maintained at 5. During the addition of $HAuCl_4$ to AB at room temperature, we noted the exothermic nature of the reduction, and white fumes evolved accompanied by a color change of the reaction mixture from yellow to red. However, we found that the reaction did not proceed to completion within 3 h. Even after 6 h, unreacted metal salts were recovered.

We also carried out reactions of three different copper salts, namely, $Cu(NO_3)_2$, $CuCl_2$, and $Cu(OCOCH_3)_2$ with AB in a molar ratio of 1:5 in each case. The metal salts were added in small batches to AB. In case of reaction with $Cu(NO_3)_2$, we noted a fire accompanied by evolution of white fumes when the salt came into contact with AB indicating high exothermicity of the reaction. In all the three cases, red nanopowders of Cu(0) were obtained. The particle sizes of Cu nanoparticles were found to be 4.7 ± 2.1, 4.3 ± 1.8, and 5.1 ± 2.4 nm in the reactions with $CuCl_2$, $Cu(NO_3)_2$, and $Cu(OCOCH_3)_2$, respectively. The BF TEM images of these samples are shown in Figures 2a, 2b, and 2c. All of these samples were

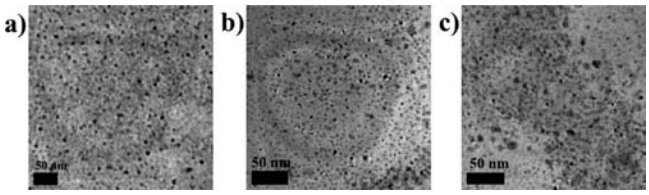


**Figure 2.** TEM BF image of Cu nanoparticles prepared by using different metal precursor: (a) copper chloride, (b) copper nitrate, (c) copper acetate.

found to be air and moisture stable since the particles are embedded in $BNH_x$ polymer. Thus, irrespective of the starting copper salt, the particle sizes of the resulting Cu nanoparticles were found to be nearly the same.

**2. Synthesis of Monometallic Nanoparticles via Reduction of Metal Salts Using AB, DMAB, and TMAB.** *a. Silver Nanoparticles.* Silver nanoparticles were prepared via the solid state route starting from $AgNO_3$ using AB, DMAB, and TMAB as the reducing agents. In a previous communication, we reported the preparation of Ag nanoparticles from $AgNO_3$ and AB.[14] The reaction was found to be highly exothermic, and it was accompanied by evolution of white fumes. Spherical Ag nanoparticles embedded in a polymer matrix were obtained. In a similar manner, Ag nanoparticles were prepared using DMAB as the reducing agent. Because of the low melting point of DMAB (37 °C), under the reaction conditions (60 °C), it became a melt. When $AgNO_3$ was added to this melt in small batches, an exothermic reaction took place accompanied by the colorless mixture turning yellow indicating the formation of Ag nanoparticles. In this reaction as well, white fumes were noted. Reduction of $Ag^+$ in this case was as fast as in the reaction with AB. After 3 h of vigorous stirring during which time the reaction proceeded to completion, dry THF was added to remove any unreacted DMAB from the reaction mixture. Finally, the dark yellow colored metal nanopowder was isolated and dried in vacuo. The BF TEM image (Figure 3a) of this sample showed the presence


dx.doi.org/10.1021/ic3021436 | Inorg. Chem. 2012, 51, 13023−13033

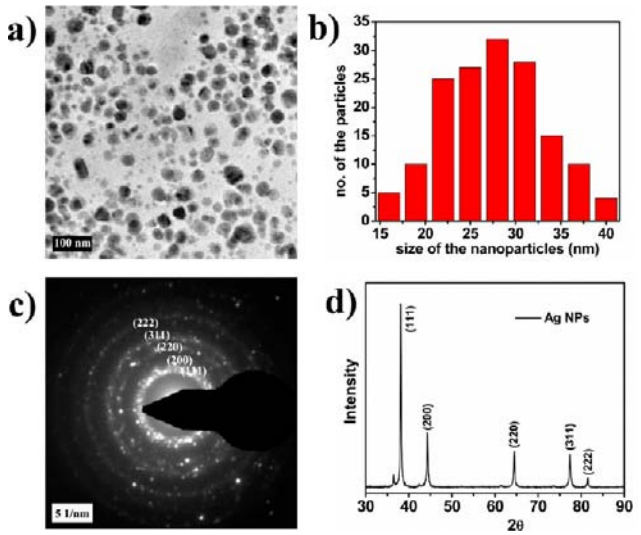


**Figure 3.** Ag nanoparticles prepared by DMAB as the reducing agent: (a) TEM BF image, (b) particle size distribution histogram, (c) SAED pattern, (d) powder XRD pattern.

of mostly spherical nanoparticles with a few irregularly shaped particles. The particles were however, found to be much larger in size as well as polydisperse in nature in this case. The average particle size was calculated to be 27.6 ± 7 nm (particle size distribution histogram, Figure 3b). The presence of FCC Ag(0) was confirmed from the corresponding SAED pattern (Figure 3c) which showed rings due to the (111), (200), (220), (311), and (222) planes. The powder XRD pattern (Figure 3d) gave peaks corresponding to FCC Ag(0) (JCPDS-870720).

In contrast to the reducing agents AB and DMAB, when TMAB was used, the reaction was carried out at room temperature since at higher temperatures TMAB undergoes sublimation. The reduction in this case was much slower in comparison to the other two. In addition, since the reaction was less exothermic, appreciable gas evolution was not observed. The reaction proceeded to completion after nearly 12 h of vigorous stirring. The dark yellow Ag nanopowder was isolated as in the previous case. Unlike the case of DMAB, only spherical nanoparticles with a narrow size distribution were realized when TMAB was employed as the reducing agent. Using TEM we found that the average particle size to be 2.7 ± 1 nm. The powder XRD pattern of the sample conformed to the FCC phase of Ag. TEM and XRD data have been deposited in the Supporting Information. In case of AB mediated reduction process, the $BNH_x$ polymer that is formed during the reaction halts the growth of the particles and also acts as a stabilizer. However, in the case of DMAB and TMAB mediated reactions, there is no possibility of polymer formation, and hence the amine groups present in these amine-boranes provide the stability for the particles. The FTIR spectra of Ag nanopowder obtained by DMAB reduction shows both N−H and C−H stretching vibrations of dimethyl amine group at 3094 and 2766 $cm^{-1}$, respectively, in addition to the B−N and C−N stretching vibrations. No B−H stretching vibration was noted in this case. This is due to the solvolysis of the B−N bond during washing of the powder using THF. However, both C−H and B−H stretching vibrations were noted in case of Ag nanopowder obtained in the reaction with TMAB which further supports our proposal that the amine group serves as the stabilizing group for the nanoparticles. The IR spectra of the samples as well as pristine amine-boranes have been deposited in the Supporting Information.

*b. Gold Nanoparticles.* Reaction of DMAB with $HAuCl_4$ resulted in a color change from yellow to red. The red powder was washed several times with dry THF to remove any unreacted DMAB. Upon drying the residue after removal of THF, a red sticky material was obtained. Characterization of the sample was established using TEM and powder XRD, and the data have been deposited in the Supporting Information. In the XRD pattern, we also noted peaks of small intensities assignable to the chloride salt of dimethylamine.

Reaction of TMAB with $HAuCl_4$ on the other hand, did not result in an immediate color change but after about 30 min, red coloration developed which darkened with time. The dark red colored powder was isolated after 12 h and washed with dry THF several times and then dried in vacuo. The BF TEM image (Figure 4a) showed nanoparticles that were much

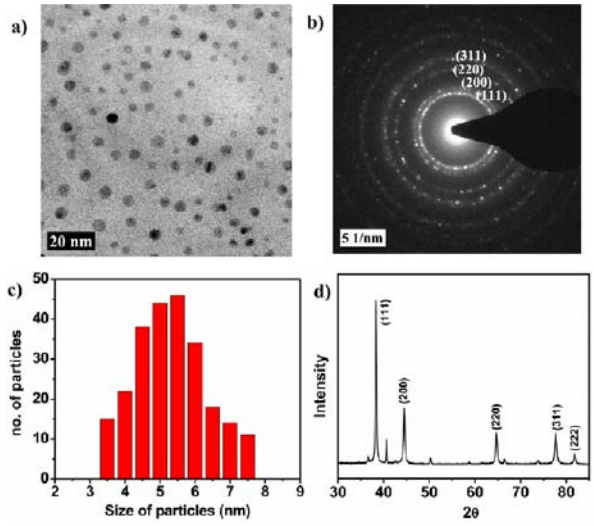


**Figure 4.** Au nanoparticles prepared by TMAB as the reducing agent: (a) TEM BF image, (b) SAED pattern, (c) size distribution histogram, (d) powder XRD pattern.

smaller compared to those obtained using DMAB as the reducing agent. In this case as well, the SAED pattern (Figure 4b) showed a ring pattern which could be indexed to the FCC phase of Au(0). The average particle size calculated from the TEM image is 5.3 ± 1.4 nm (Figure 4c). The powder XRD pattern (Figure 4d) corroborated the TEM data.

*c. Copper Nanoparticles.* In the preparation of Cu nanoparticles from $Cu^{2+}$ using AB as the reducing agent, we noted that $BNH_x$ polymer that is formed during the reaction plays a dual role by stabilizing the particles toward agglomeration as well as preventing the particles from getting oxidized.[14] Cu(0) in the nanosize regime is highly prone to oxidation and is oxidized within seconds of exposure to air to form $Cu_2O$. The XPS spectrum of Cu nanoparticles (Figure 5) obtained in our experiments exhibited two binding energy peaks at 932.1 and 952.1 eV which could be attributed to the $2p_{3/2}$ and $2p_{1/2}$ spin system of Cu(0). This rules out the presence of any oxide.

When we used DMAB as the reducing agent, we noted an immediate color change from brown to brick red. No further color change was observed even after prolonged stirring under $N_2$ atmosphere. Exposure of this reaction mixture to air


dx.doi.org/10.1021/ic3021436 | Inorg. Chem. 2012, 51, 13023−13033

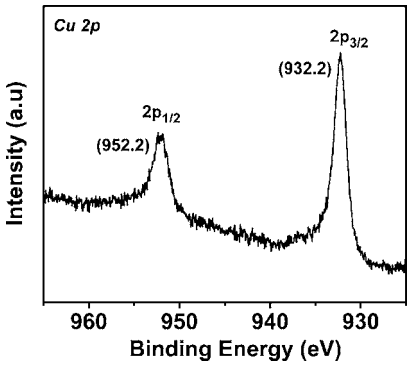


**Figure 5.** XPS spectrum of copper nanoparticles.

rendered the brick red powder green within about 1 h suggesting that oxidation had taken place. The powder XRD pattern of the brick red powder (see Supporting Information) evidenced the presence of copper hydride. Thus, DMAB being a weaker reducing agent could reduce $Cu^{2+}$ to only $Cu^{+}$ but not to Cu(0). This is further reiterated by the lower reduction potential of the $Cu^{2+}/Cu^{0}$ systems compared to the higher congeners of the group. Further characterization of the sample was not possible because of the unstable nature of copper hydride. Use of TMAB, a much weaker reducing agent, did not lead to any reduction of $Cu^{2+}$ species as expected. Unreacted $CuCl_2$ and TMAB were recovered even after prolonged stirring of the reaction mixture.

*d. Palladium Nanoparticles.* Addition of $Pd(OCOCH_3)_2$ to AB in small batches followed by vigorous stirring of the mixture resulted in a color change from brown to black. During the addition, we noted evolution of white fumes. The black powder was isolated after 3 h of stirring and then washed repeatedly with dry THF. A TEM sample was made by redispersing a small quantity of the powder in THF by sonication followed by drop coating on a TEM grid. The BF TEM image revealed the presence of highly monodisperse, well separated Pd nanoparticles of 5.3 ± 1.2 nm (Figure 6a). The SAED pattern (Figure 6b) showed rings corresponding to the FCC phase of Pd(0). The size distribution histogram is shown in Figure 6c. The powder XRD pattern (Figure 6d) showed peaks corresponding to Pd(0). However, all the peaks had a shoulder on the left (lower $2\theta$ values) which could be assigned to $PdH_x$.[24] We earlier reported that hydrolysis of AB with Pd(0) nanopowder results in the generation of active hydrogen atoms. Some of the active hydrogen atoms combine with one another resulting in $H_2$ evolution and some diffuse into the Pd lattice to give $PdH_x$. When hydrogen atoms diffuse into the Pd lattice, the lattice expands which could be established by powder XRD.[25]

Reduction of $Pd(OCOCH_3)_2$ using DMAB gave a similar observation as that of the reaction with AB. The reaction was complete within 3 h. Characterization of this sample was established by TEM and XRD (data deposited in Supporting Information). Compared to the other monometallic systems, in case of preparation of Pd nanoparticles using DMAB, we noted that the particles are quite polydisperse. The very broad nature of the powder XRD peaks precluded unambiguous assignment of both Pd(0) and $PdH_x$ in this sample. Reduction of Pd(II) using TMAB was found to be much slower in comparison to those with AB or DMAB. This resulted in well separated spherical nanoparticles. The sample was characterized using TEM and XRD (data deposited in Supporting Information). Once again in this case, the broad nature of the powder XRD peaks rendered unambiguous assignment of both Pd and $PdH_x$.

*e. Iridium Nanoparticles.* Reaction of AB with $H_2IrCl_6$ as the Ir precursor did not result in any gas evolution or color change from black. After about 1 h of stirring, a gradual color change to yellow was observed. Unlike the other cases, herein we noted that addition of the metal precursor in a single batch did not make a difference. The reaction proceeded to completion in about 6 h. The yellow powder that resulted was washed several times with THF and dried in vacuo. The BF TEM image (Figure 7a) of the sample revealed the presence of highly monodisperse Ir nanoparticles of 1−2 nm. The HRTEM image (Figure 7b) showed lattice fringes with a *d* spacing of 2.23 Å due to the (111) plane of FCC Ir(0) evidencing the

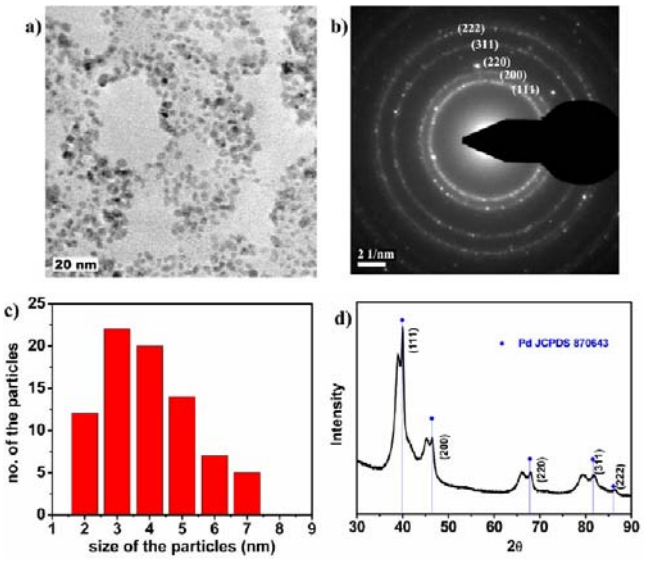


**Figure 6.** Pd nanoparticles prepared by AB as the reducing agent: (a) TEM BF image, (b) SAED pattern, (c) size distribution histogram, (d) powder XRD pattern.

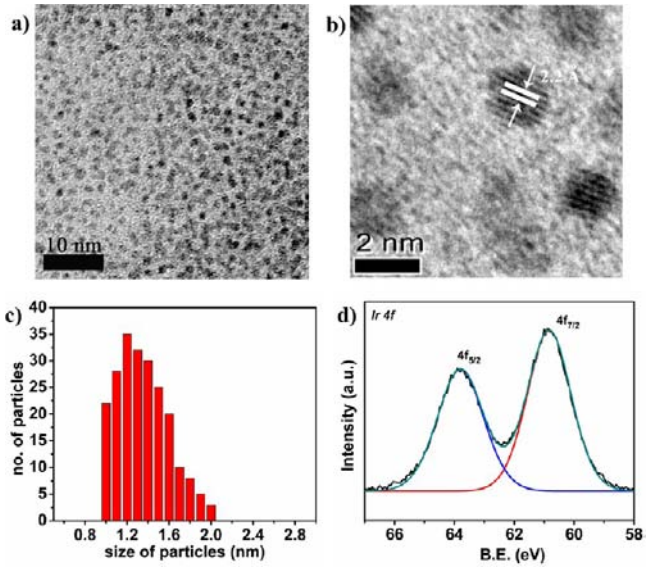


**Figure 7.** Ir nanoparticles prepared by AB as the reducing agent: (a) TEM BF image, (b) HRTEM image, (c) size distribution histogram, (d) XPS spectrum.


dx.doi.org/10.1021/ic3021436 | *Inorg. Chem.* 2012, 51, 13023−13033

crystalline nature of the sample. The average particle size obtained from the size histogram is 1.4 ± 0.3 nm (Figure 7c). Iridium nanoparticles in this size regime should be highly susceptible toward oxidation. On the contrary, exposure of the sample to air for several months did not result in oxidation of Ir. This suggests that the particles are well protected, as in case of Cu, Ag, and Au embedded in $BNH_x$ polymer. To rule out surface oxidation of the particles, we recorded the XPS spectrum (Figure 7d) of Ir nanoparticles which showed the presence of two peaks at 60.8 and 63.9 eV due to $4f_{7/2}$ and $4f_{5/2}$ spin systems of iridium, respectively. These peaks could be attributed to Ir(0).[26] The XRD pattern of the sample was devoid of any peaks which could be ascribed to the very small size of the particles. A similar behavior was reported for noble metal nanoparticles where a set of well-defined diffraction peaks disappeared because of transition from large size domain to atomic scale clusters.[27−30] Heat treatment of the powder in a sealed tube under $N_2$ atmosphere at 300 °C for 14 h rendered a color change from yellow to black. Transmission electron microscopy evidenced complete agglomeration of the particles. Powder XRD pattern, however, exhibited peaks due to the FCC phase of Ir(0) (data deposited in the Supporting Information).

Reduction of $H_2IrCl_6$ using DMAB and TMAB afforded similar observations as in the case of the reaction with AB. In both of these reactions, Ir nanoparticles that were obtained did not show any indications of either surface or bulk oxidation. The characterization data of these samples have been deposited in the Supporting Information. Interestingly, in all the three reactions, we did not find any single region where particles of more than 3 nm were present. Although there have been several reports on the synthesis of Ir nanoparticles in solution, in most cases the particles were found to be more than 2 nm and in a few cases, the particles were found to be unstable under ambient conditions.[31−36] In such cases, surface oxidation or complete oxidation of the particles took place resulting in the formation of $IrO_x$. Gram scale preparation of air stable Ir nanoparticles (∼ 1−2 nm) reported herein via solid state route is unprecedented.

**3. Synthesis of Bimetallic Nanoparticles via Reduction of Metal Salts Using AB, DMAB, and TMAB.** *a. AuCu Alloy Nanoparticles.* The successful synthesis of several monometallic nanoparticles, for example, Cu, Ag, Au, Pd, and Ir with narrow size distribution prompted us to explore this new synthetic methodology toward the preparation of bimetallic systems. Traditionally, alloys in the bulk state are obtained by metallurgical techniques involving high temperature processes. Recently, Sakurai and co-workers synthesized AuAg alloy nanomaterials by solid state grinding in presence of chitosan and a base, wherein chitosan acts as both reducing agent and a capping agent.[37] To the best of our knowledge, solid state synthetic routes for bimetallic nanostructured materials are scarce.

Gold and copper form a solid solution in the entire composition range. Several solution phase syntheses of nanocrystalline AuCu bimetallic systems such as AuCu, $AuCu_3$, or $Au_3Cu$ have been reported.[38,39] The AuCu alloy systems have found several applications including catalysis.[40−42] Addition of an equimolar mixture consisting of $HAuCl_4$ and $Cu(NO_3)_2$ to AB (1:1:10) kept at 60 °C in a batch wise manner resulted in a fire followed by evolution of white fumes. The reaction mixture turned reddish brown. The reaction was continued for 6 h after which time a dark red powder was obtained. The powder was washed with dry THF several times and dried in vacuo. The BF TEM image (Figure 8a) showed the presence of 2−5 nm spherical nanoparticles. The high angle

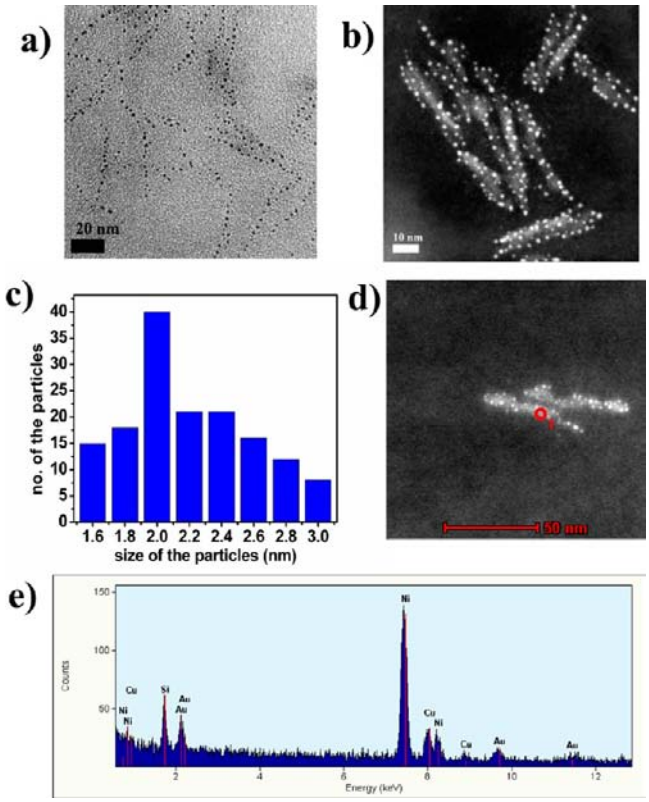


**Figure 8.** Characterization of AuCu alloy nanoparticles: (a) TEM BF image, (b) HAADF image, (c) size distribution histogram, (d) HAADF-STEM image showing the analyzed nanoparticles with marking, (e) EDS spectrum obtained from the nanoparticles marked in panel d.

annular dark-field (HAADF) image also showed the presence of well separated particles (Figure 8b). The size distribution histogram (Figure 8c) gave an average particle size of 2.2 ± 0.5 nm indicating that the sample is nearly monodisperse. We attempted to obtain high resolution images; however, the sample began drifting under the electron beam at high magnification. This could be due to the degradation of the $BNH_x$ polymer which forms under the reaction conditions and embeds the particles. We employed scanning transmission electron microscopy (STEM)-energy dispersive X-ray spectroscopy (EDS) technique to establish the composition of the sample. Figures 8d and e show the HAADF image with the individual particle marked in this case that was analyzed and the EDS spectrum, respectively. The EDS spectrum showed the presence of both Au and Cu within the same particle which proves without any ambiguity the bimetallic nature of the particles.

The powder XRD pattern of AuCu bimetallic system is composed of a single phase FCC alloy structure with no probable impurity of $CuO_x$ or phase segregated metals (Figure 9a). Figure 9b shows an enlarged version of the XRD pattern where only the (111) and the (200) peaks are highlighted. It is very clear that these two peaks are shifted slightly to the higher $2\theta$ values with respect to those of pure Au(0) (JCPDS-040784). This angular shift corroborates alloy formation between Au and Cu and suggests a lattice contraction resulting


dx.doi.org/10.1021/ic3021436 | Inorg. Chem. 2012, 51, 13023−13033

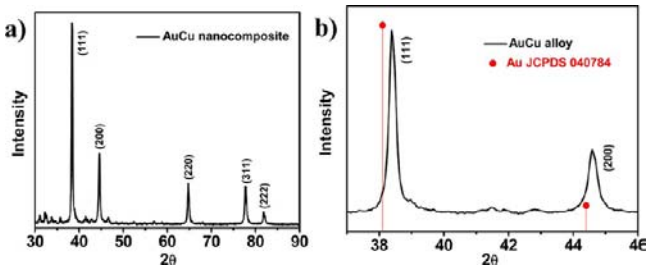


**Figure 9.** (a) Powder XRD pattern of AuCu alloy nanoparticles, (b) zoomed-in region showing the (111) and (200) reflections; vertical line corresponds to the (111) and (200) peak positions for Au.

from the incorporation of smaller Cu into the Au FCC lattice.[43] The lattice parameter calculated for AuCu system herein is 4.04 Å which is smaller than that of pure Au(0), 4.09 Å.

*b. AgCu Alloy Nanoparticles.* We further prepared AgCu bimetallic system in a similar manner to that of AuCu starting from $AgNO_3$ and $Cu(NO_3)_2$. The reaction was much more violent since the metal precursors in this case are both nitrates. Reduction of the metal salts resulted in a color change from blue to black. The powder was washed with dry THF and dried in vacuo. The BF TEM image revealed the presence of 5−10 nm particles embedded within a polymer matrix (Figure 10a). From the size distribution histogram it can be inferred that the sample consists of 8.1 ± 1.3 nm particles (Figure 10b). The crystalline nature of the particles was apparent from the HRTEM image which showed lattice fringes corresponding to the (111) plane of FCC Ag (Figure 10c). However, the *d* spacing calculated from the FFT pattern is 2.27 Å which is lower than that of pure Ag(0) (2.36 Å). The HAADF image of the sample is shown in Figure 10d. The EDS spectrum obtained from a single particle (marked in Figure 10e) shows coexistence of signals from both Ag and Cu confirming the bimetallic nature of the particles (Figure 10f). The powder XRD pattern of the sample showed the presence of a single phase FCC AgCu alloy system corroborating the other supporting data (see Supporting Information). No copper oxide or phase segregated metal was found. In the preparation of AgCu alloy nanoparticles, powder X-ray diffraction pattern of a sample recorded after 3 h of reaction time revealed peaks of AgCu alloy together with Cu nanoparticles (powder XRD pattern of the sample recorded after 3 h of reaction time has been deposited in the Supporting Information). Continuation of the reaction for an additional 3 h resulted in its completion and no monometallic nanoparticles were found.

## DISCUSSION

Considering all the advantages of amine-boranes, we attempted synthesis of monometallic and bimetallic nanoparticles in the solid state. The solid state synthetic route is an exciting prospect since it excludes use of volatile organic solvent which has many adverse effects on the environment. The nucleation and the growth processes involved in this synthetic protocol are however of complex nature because of the heterogeneity present in the system. Thus, to get a comprehensive

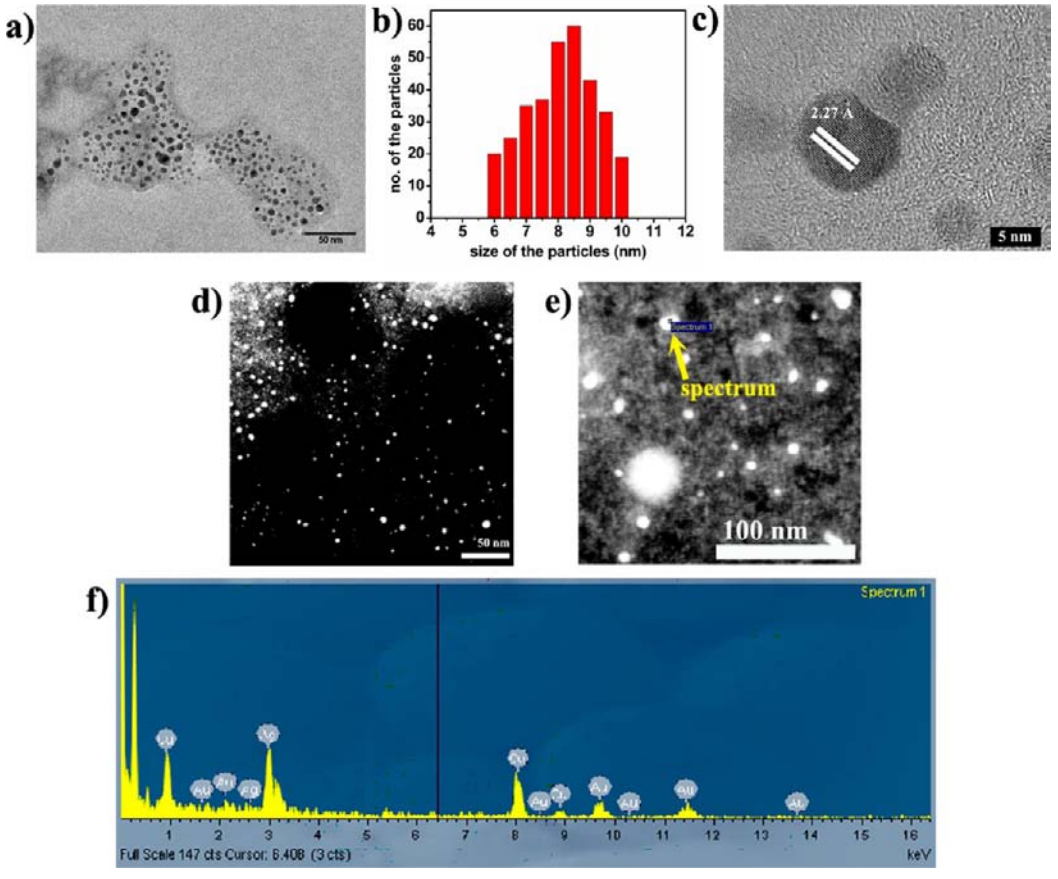


**Figure 10.** Characterization of CuAg alloy nanoparticles: (a) TEM BF image, (b) size distribution histogram, (c) HRTEM image, (d) HAADF image, (e) HAADF-STEM images showing the analyzed nanoparticles with marking, (e) EDS spectrum obtained from the nanoparticles marked in panel e.


dx.doi.org/10.1021/ic3021436 | *Inorg. Chem.* 2012, 51, 13023−13033

understanding of the nucleation and growth processes and in turn their influence on the size as well as the size distribution of the nanoparticles, we chose three different amine-borane systems: ammonia borane (AB), dimethylamine borane (DMAB), and trimethylamine borane (TMAB) as the reducing agents in our study. The reducing ability of the alkylamine boranes decreases with increase of the alkyl substituents on nitrogen and the order follows AB > DMAB > TMAB.[19] Thus, the kinetics of the reduction would be expected to be fastest for AB followed by DMAB and then TMAB. Primary and secondary amine-boranes are thermally unstable at about 80 °C at which point rupture of the intramolecular hydrogen bonding network sets in followed by decomposition resulting in the formation of several B- and N-based solid products which could act as stabilizing agents for metal nanoparticles.[44−46]

Reaction of AB with various metal salts led to instantaneous color change and reduction of the metal ions. All the reactions were found to be exothermic and resulted in evolution of white fumes during the addition of metal salt to AB. In particular, the reduction of metal nitrates was the most exothermic and resulted in small flames, in addition. We propose that the reaction pathway in these cases involves the intermediacy of $NH_4NO_3$ (the heat liberated in these reactions decomposes $NH_4NO_3$). This proposal is based on the powder XRD pattern of the raw products (before washing) which showed peaks corresponding to $NH_4Cl$ together with those of metal(0) in case of chloride salts. In case of metal acetates as metal precursors, the reactions proceed through the intermediacy of $NH_4OCOCH_3$ which undergoes decomposition under the reaction conditions. Finally metal nanopowders were obtained after washing with dry THF which resulted in removal of the ammonium salt along with the unreacted amine-boranes. A set of controlled experiments revealed that the process of addition of metal salts to AB is a crucial step to achieve small size with narrow size distribution of particles. Batch-wise addition as opposed to sudden addition of metal salt to AB generates fewer nuclei at a time that are always surrounded by adequate amount of capping agent during the nucleation, followed by controlled growth that leads to monodisperse nanoparticles. Further experiments by employing different ratios of AB to metal salt show that the ratio should be at least 5 for reaction completion resulting in monodisperse nanoparticles as the product. Thus, it is clearly evident that once AB reduces the metal salt, $BNH_x$ polymer produced in situ plays the most decisive role to control the growth process and hence control the size of the thus generated nanoparticles. Only agglomerated nanoparticles were realized in the absence of polymer. Next, we examined the effect of counteranions using copper salts with different anions, for example, nitrate, chloride, and acetate. The reactions in reference to nucleation and growth processes were unaffected; the particle size and the size distribution were similar in all these three cases.

In the preparation of iridium nanoparticles starting from chloroiridic acid ($H_2IrCl_6$), the reduction proceeded very slowly compared to the other systems (i.e., Ag, Au, Cu, and Pd), but the particles that resulted from this reaction were quite small (≤2 nm). This observation confirms our proposition that the kinetics of reduction should be sufficiently slow to match the rate of generation of the stabilizer, here the $BNH_x$ polymer. When there is sufficient stabilizer at the time that nuclei are formed, they get protected and the growth process is slowed down or halted which results in ultrasmall nanoparticles, and this also results in monodispersity of the sample. It has been well documented in the literature that once nuclei are formed, they grow via diffusion and result in nanoparticles wherein the presence of the capping agent within the medium in which the reaction is conducted prevents their growth toward bulk.[47−50] In contrast, in the solid state, diffusion is negligible; however, formation of metal nuclei could take place on the surface of the macroscopic solid particles of the reagents in a facile manner where diffusion is much easier than in the bulk solid. We believe that once nuclei are formed, only those nuclei that are close to one another would participate in the growth process and result in nanoparticles. Therefore, it is apparent that the rate of formation of stabilizing agent should be higher or comparable to the rate of formation of metal nuclei to realize a controlled growth process. In case of preparation of Ir nanoparticles using AB, the nucleation and $BNH_x$ polymer formation proceed hand in hand, and as a result extremely small particles (1.4 ± 0.3 nm) that are highly monodisperse are obtained.

When DMAB and TMAB were used as reducing agents, the amine groups present in these reagents act as stabilizing agents. Magnetic and noble metal nanoparticles stabilized by primary, secondary, and tertiary amine moieties as capping agents have been reported in the literature.[51−53] When a large number of nuclei are formed, an effective capping agent is needed to control the growth process such that small particles and monodispersity could be achieved. Dimethylamine borane, with reducing ability that is nearly comparable to that of AB, produces a large number of nuclei; it also provides $-Me_2NH$ moiety as a stabilizer for nanoparticles, which however, is not as effective as $BNH_x$ polymer formed in the reaction with AB. As a result, the nuclei formed enter into an uncontrolled growth process and finally give large particles that are polydisperse. Further, because of the low melting point of DMAB (37 °C), it is present as a melt under the reaction conditions (60 °C); thus, the interparticle diffusion process cannot be completely neglected. When TMAB is used as a reducing agent, only a few nuclei are produced at a time. Since the reaction is conducted in the solid state wherein negligible diffusion takes place, growth of nanoparticles is restricted from the fewer nuclei that are available resulting in smaller sized particles. In addition, trimethylamine ($-Me_3N$) provided by TMAB acts as a better stabilizing agent in comparison to dimethylamine because of its bulkiness; therefore, nanoparticles obtained are smaller in size. A schematic representation of the nucleation, growth, and formation of nanoparticles using AB, DMAB, and TMAB is shown in Scheme 1.

We noted that the reaction of metal nitrate with AB is highly exothermic. The heat evolved in this reaction provides the required amount of energy for proper mixing of the constituents thus facilitating the reaction at much milder conditions (at 60 °C herein). Additionally, because of the simultaneous formation of $BNH_x$ polymer which acts as a stabilizer, the growth of the bimetallic particles gets restricted effectively thereby resulting in particles in the nanosize regime and also in monodispersity. Using this methodology, we have been successful in synthesizing AuCu and AgCu bimetallic systems and established their alloy nanostructures unambiguously using microscopy and XRD techniques.

Although a large body of literature is available regarding the synthesis of metallic as well as bimetallic alloy nanopaticles, there has been no focus on the development of new synthetic routes for metal nanoparticles in a sustainable pathway. For a process to be green, it is obligatory for the preparative route to

**Scheme 1. Schematic Representation of Nucleation and Growth of Metal Nanoparticles during the Reduction of Metal Salts Using AB, DMAB, and TMAB as the Reducing Agent in the Solid State**

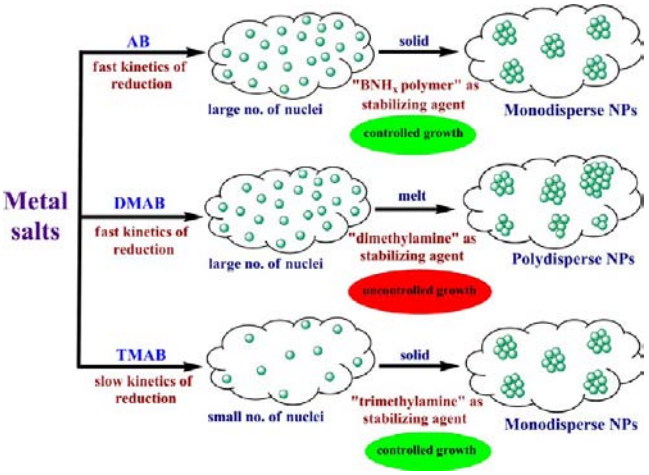


be sustainable for a long time. In brief, for a process to be really sustainable, the following criteria have to be met: (i) the process should be carried out under mild conditions if possible, at ambient conditions, (ii) no solvent should be involved, (iii) reagents which play multiple role should be employed such that formation of byproduct(s) can be eliminated (i.e., atom economy), (iv) it should yield particles with narrow size distribution, and (v) it should be easily scalable. Herein, we used amine-boranes as reducing agents, which not only reduce the metal salts in the solid state but also generate B−N based compounds simultaneously during the reduction which essentially acts as a stabilizing agent to stabilize the nanoparticles formed. Amine-borane plays a dual role: it acts as a reducing agent and also as a precursor for the stabilizing agent, that is, it maximizes the materials efficiency for the conversion of reagent to desirable product, hence eliminates the formation of byproduct, thus, bringing out atom economy to the overall process. Moreover, all the reductions were carried out at mild temperatures and/or room temperature. In addition, we scaled up the synthesis of the monometallic as well as the bimetallic systems to gram quantities successfully without any change in the particle size or the size distribution compared to the small scale reactions. Hence, we believe that the solid state synthetic route we have developed herein can pave a way towards sustainability.

## CONCLUSIONS

In summary, we have developed an atom economy solid state synthetic route toward the preparation of monometallic and bimetallic alloy nanoparticles by employing amine-boranes as the reducing agent. During the reduction, amine-borane reduces the metal salt and simultaneously generates the stabilizing agent ($BNH_x$ polymer in case of AB whereas complexing amine in case of DMAB and TMAB) in situ which plays the most decisive role by controlling the growth process and affords nearly monodisperse nanosized particles. Several controlled experiments revealed that during the reduction process, the presence of an optimum amount of amine-borane is necessary to complete the reduction as well as to generate adequate amount of stabilizer to realize monodisperse nanoparticles. The rate of formation of metal nuclei should be comparable to the rate of generation of the stabilizing agent to realize the smallest possible size of the particles with a narrow size distribution. Reduction process of $H_2IrCl_6$ to Ir nanoparticles was the slowest among the systems studied; in this case, nucleation kinetics matches best with the rate of polymer generation and leads to a controlled growth and hence highly monodisperse nanoparticles of 1−2 nm which further reiterates our proposition. Considering all the metal systems studied herein, AB and TMAB produce smaller size particles whereas DMAB produces polydisperse particles which are larger in size too. Thus, a comprehensive understanding of the nucleation and the growth processes of metal nanoparticles in the solid state obtained herein by employing different amine-boranes of differing reducing strength offers to choose the reducing agent judiciously to obtain the best possible results. By exploiting the exothermic nature of the AB mediated reduction with metal nitrate as the precursor we also successfully synthesized a CuAu and CuAg alloy nanocomposite of 2−10 nm diameter. The heat evolved during the course of reduction provides sufficient energy required to mix the constituent elements leading to alloy nanostructure and therefore prevents the necessity of harsh reaction conditions. The solid state route developed here offers a simple and convenient pathway to prepare metal as well as alloy nanostructures at the gram scale, and thus should find a broad application as a versatile and energy-efficient synthetic method which finally leads toward sustainability.

## ASSOCIATED CONTENT

### Supporting Information

Characterization data (TEM, XRD, and IR spectroscopy) of the samples. This material is available free of charge via the Internet at http://pubs.acs.org.

## AUTHOR INFORMATION

### Corresponding Author

*E-mail: jagirdar@ipc.iisc.ernet.in.

### Author Contributions

The manuscript was written through contributions of all authors. All authors have given approval to the final version of the manuscript.

### Notes

The authors declare no competing financial interest.

## ACKNOWLEDGMENTS

We gratefully acknowledge financial support from the Council of Scientific & Industrial Research, India. We also thank the Indian Institute of Science for funding the procurement of a 200 kV TEM and the institute XRD facility for the powder X-ray diffraction data.

## REFERENCES

(1) Rogach, A. L.; Talapin, D. V.; Shevchenko, E. V.; Kornowski, A.; Haase, M.; Weller, H. *Adv. Funct. Mater.* **2002**, *12*, 653.
(2) (a) Roucoux, A.; Schulz, J.; Patin, H. *Chem. Rev.* **2002**, *102*, 3757. (b) Klabunde, K. J.; Richards, R. M. In *Nanoscale Materials in Chemistry*, 2nd ed; Wiley-VCH Publishers: New York, 2009.
(3) Cushing, B. L.; Kolesnichenko, V. L.; O'Connor, C. J. *Chem. Rev.* **2004**, *104*, 3893.
(4) Daniel, M.-C.; Astruc, D. *Chem. Rev.* **2004**, *104*, 293.
(5) Sheldon, R. A. *Green Chem.* **2005**, *7*, 267.
(6) Quiñones, L.; Grazul, J.; Martínez-Iñesta, M. M. *Mater. Lett.* **2009**, *63*, 2684.

(7) Dahl, J. A.; Maddux, B. L. S.; Hutchison, J. E. *Chem. Rev.* **2007**, *107*, 2228.
(8) Wostek-Wojciechowska, D.; Jeszka, J. K.; Amiens, C.; Chaudret, B.; Lecante, P. *J. Colloid Interface Sci.* **2005**, *287*, 107.
(9) Debnath, D.; Kim, S. H.; Geckeler, K. E. *J. Mater. Chem.* **2009**, *19*, 8810.
(10) Park, J.; Joo, J.; Kwon, S. G.; Jang, Y.; Hyeon, T. *Angew. Chem., Int. Ed.* **2007**, *46*, 4630.
(11) Staubitz, A.; Robertson, A. P. M.; Manners, I. *Chem. Rev.* **2010**, *110*, 4079.
(12) Zheng, N.; Fan, J.; Stucky, G. D. *J. Am. Chem. Soc.* **2006**, *128*, 6550.
(13) Kalidindi, S. B.; Sanyal, U.; Jagirdar, B. R. *ChemSusChem* **2011**, *4*, 317.
(14) Kalidindi, S. B.; Sanyal, U.; Jagirdar, B. R. *Inorg. Chem.* **2010**, *49*, 3965.
(15) Kalidindi, S. B.; Indirani, M.; Jagirdar, B. R. *Inorg. Chem.* **2008**, *47*, 7424.
(16) Kalidindi, S. B.; Vernekar, A. A.; Jagirdar, B. R. *Phys. Chem. Chem. Phys.* **2009**, *11*, 770.
(17) Yan, J. M.; Zhang, X. B.; Han, S.; Shioyama, H.; Xu, Q. *Angew. Chem., Int. Ed.* **2008**, *47*, 2287.
(18) Yan, J. M.; Zhang, X. B.; Akita, T.; Haruta, M.; Xu, Q. *J. Am. Chem. Soc.* **2010**, *132*, 5326.
(19) (a) Hutchins, R. O.; Learn, K.; Nazer, B.; Pytlewski, D.; Pelter, A. *Org. Prep. Proced. Int.* **1984**, *16*, 335. (b) Staubitz, A.; Robertson, A. P. M.; Sloan, M. E.; Manners, I. *Chem. Rev.* **2010**, *110*, 4023.
(20) Ramachandran, P. V.; Gagare, P. D. *Inorg.Chem.* **2007**, *46*, 7810.
(21) Kalidindi, S. B.; Joseph, J.; Jagirdar, B. R. *Energy Environ. Sci.* **2009**, *2*, 1274.
(22) JCPDS 04-0783.
(23) JCPDS 04-0784.
(24) Phan, T. H.; Schaak, R. E. *Chem. Commun.* **2009**, 3026.
(25) Jose, D.; Jagirdar, B. R. *Int. J. Hydrogen Energy* **2010**, *35*, 6804.
(26) Bernadi, F.; Scholten, J. D.; Fecher, G. H.; Dupont, J.; Morais, J. *Chem. Phys. Lett.* **2009**, *479*, 113.
(27) Wang, T.; Hu, X.; Dong, S. *Chem. Commun.* **2008**, 4625.
(28) Wu, Z.; Chen, J.; Jin., R. *Adv. Funct. Mater.* **2011**, *21*, 177.
(29) Kim, Y.; Ohshima, K.; Higashimine, K.; Uruga, T.; Takata, M.; Suematsu, H.; Mitani, T. *Angew. Chem., Int. Ed.* **2006**, *45*, 407.
(30) Chen, S.; Kimura, K. *Langmuir* **1999**, *15*, 1075.
(31) Ott, L. S.; Hornstein, B. J.; Finke, R. G. *Langmuir* **2006**, *22*, 9357.
(32) Stowell, C. A.; Korgel, B. A. *Nano Lett.* **2005**, *5*, 1203.
(33) Özkar, S.; Finke, R. G. *Langmuir* **2003**, *19*, 6247.
(34) Dupont, J.; Fonseca, G. S.; Umpierre, A. P.; Fichtner, P. F. P.; Teixerira, S. R. *J. Am. Chem. Soc.* **2002**, *104*, 4228.
(35) Lin, Y.; Finke, R. G. *J. Am. Chem. Soc.* **1994**, *116*, 8335.
(36) Bönnemann, H.; Brijoux, W.; Brinkmann, R.; Dinjus, E.; Jouβen, T.; Korall, B. *Angew. Chem., Int. Ed.* **1991**, *30*, 1312.
(37) Murugadoss, A.; Kai, N.; Sakurai, H. *Nanoscale* **2012**, *4*, 1280.
(38) Schaak, R. E.; Sra, A. K.; Leonard, B. M.; Cable, R. E.; Bauer, J. C.; Han, Y.-F.; Means, J.; Teizer, W.; Vasquez, Y.; Funck, E. S. *J. Am. Chem. Soc.* **2005**, *127*, 3506.
(39) Sra, A. K.; Schaak, R. E. *J. Am. Chem. Soc.* **2004**, *126*, 6667.
(40) Llorca, J.; Dominguez, M.; Ledesma, C.; Chimentao, R. J.; Medina, F.; Sueiras, J.; Angurell, I.; Seco, M.; Rossell, O. *J. Catal.* **2008**, *258*, 187.
(41) Della Pina, C.; Falletta, E.; Rossi, M. *J. Catal.* **2008**, *260*, 384.
(42) Kameoka, S.; Tsai, A. P. *Catal. Lett.* **2008**, *121*, 337.
(43) Motl, N. E.; Ewusi-Annan, E.; Sines, I. T.; Jensen, L.; Schaak, R. E. *J. Phys. Chem. C* **2010**, *114*, 19263.
(44) Baitalow, F.; Baumann, J.; Wolf, G.; Jaenicke-Rößler, K.; Leitner, G. *Thermochim. Acta* **2002**, *391*, 159.
(45) Wolf, G.; Baumann, J.; Baitalow, F.; Hoffmann, F. P. *Thermochim. Acta* **2000**, *343*, 19.
(46) Jaska, C. A.; Temple, K.; Lough, A. J.; Manners, I. *J. Am. Chem. Soc.* **2003**, *125*, 9424.
(47) Pacholski, C.; Kornowski, A.; Weller, H. *Angew. Chem., Int. Ed.* **2002**, *41*, 1188.
(48) Zheng, H.; Smith, R. K.; Jun, Y.-W.; Kisielowski, C.; Dahmen, U.; Alivisatos, A. P. *Science* **2009**, *324*, 1309.
(49) Yuk, J. M.; Park, J.; Ercius, P.; Kim, K.; Hellebusch, D. J.; Crommie, M. F.; Lee, J. Y.; Zettl, A.; Alivisatos, A. P. *Science* **2012**, *336*, 61.
(50) Niederberger, M.; Cölfen, H. *Phys. Chem. Chem. Phys.* **2006**, *8*, 3271.
(51) Chaki, N. K.; Sudrik, S. G.; Sonawane, H. R.; Vijayamohanan, K. *Chem. Commun.* **2002**, 76.
(52) Green, M.; O'Brien, P. *Chem. Commun.* **2000**, 183.
(53) Hou, Y.; Gao, S. *J. Mater. Chem.* **2003**, *13*, 1510.